Mathematical Biosciences 376 (2024) 109266

Contents lists available at ScienceDirect

Mathematical Biosciences

journal homepage: www.elsevier.com/locate/mbs

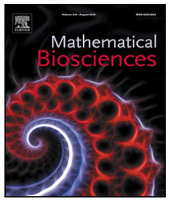

Original Research Article

Breakdown of Boltzmann-type models for the alignment of self-propelled rods

Patrick Murphy [g,1,*], Misha Perepelitsa [c,1], Ilya Timofeyev [c], Matan Lieber-Kotz [a], Brandon Islas [d], Oleg A. Igoshin [a,b,e,f]

[a] Department of Bioengineering, Rice University, Houston, TX 77005, United States of America
[b] Center for Theoretical Biological Physics, Rice University, Houston, TX 77005, United States of America
[c] Department of Mathematics, University of Houston, TX 77204, United States of America
[d] Department of Computational and Applied Mathematics, Rice University, Houston, TX 77005, United States of America
[e] Department of Chemistry, Rice University, Houston, TX 77005, United States of America
[f] Department of Biosciences, Rice University, Houston, TX 77005, United States of America
[g] Department of Mathematics and Statistics, San Jose State University, San Jose, CA 95192, United States of America

ARTICLE INFO

Dataset link: https://github.com/pmurphy12/Boltzmann-breakdown-code

Keywords:
Self-propelled rods
Kinetic models
Boltzmann equation
Cluster formation
Statistical independence
Agent-based model

ABSTRACT

Studies in the collective motility of organisms use a range of analytical approaches to formulate continuous kinetic models of collective dynamics from rules or equations describing agent interactions. However, the derivation of these kinetic models often relies on Boltzmann's "molecular chaos" hypothesis, which assumes that correlations between individuals are short-lived. While this assumption is often the simplest way to derive tractable models, it is often not valid in practice due to the high levels of cooperation and self-organization present in biological systems. In this work, we illustrated this point by considering a general Boltzmann-type kinetic model for the alignment of self-propelled rods where rod reorientation occurs upon binary collisions. We examine the accuracy of the kinetic model by comparing numerical solutions of the continuous equations to an agent-based model that implements the underlying rules governing microscopic alignment. Even for the simplest case considered, our comparison demonstrates that the kinetic model fails to replicate the discrete dynamics due to the formation of rod clusters that violate statistical independence. Additionally, we show that introducing noise to limit cluster formation helps improve the agreement between the analytical model and agent simulations but does not restore the agreement completely. These results highlight the need to both develop and disseminate improved moment-closure methods for modeling biological and active matter systems.

1. Introduction

Self-propelled rods are a fascinating class of active matter seen across both living and non-living systems [1–7]. Due to their shape, such systems are intrinsically capable of collective behavior through realignments of rods due to physical collisions [8,9] or longer-ranged hydrodynamic interactions when in a fluid [2,10]. These interactions lead to the emergence of macroscopic collective motion such as flocking, clustering, phase changes, and vortexes. Two notable biological examples of collective motion in self-propelled rods are the dynamics of rod-shaped gliding bacteria such as the soil bacterium *Myxococcus xanthus* [11–13], and the behavior of groups of cellular cytoskeletal rods (such as F-actin [4] or microtubules [5]) driven by molecular motors deposited on the surface. Collisions between *M. xanthus* cells often result in the head of the colliding cell reorienting along the length of the cell that was struck (see Fig. 1) [6]. Reorientation itself occurs on a characteristic time scale related to the ratio of the cell length to cell velocity. Microtubule collisions on a 2D surface also exhibit asymmetric realignments upon collision, with the additional possibility of the colliding microtubule stalling until the struck microtubule has passed [5].

Due to the interest surrounding systems of self-propelled rods, researchers have developed various methods of modeling them. A popular approach to studying the emergent behavior of these systems is by deriving a probabilistic description [9,14–23]. A number of heuristic mean-field models based on the notion of the mean nematic director have been considered in [15,16,24–27]. Since rod reorientation takes place only when rods collide, a more accurate approach consists in

* Correspondence to: Department of Mathematics and Statistics, San Jose State University, San Jose, CA, United States.
E-mail address: patrick.a.murphy@sjsu.edu (P. Murphy).
[1] These authors contributed equally to this project.

https://doi.org/10.1016/j.mbs.2024.109266
Received 1 February 2024; Received in revised form 23 July 2024; Accepted 3 August 2024
Available online 8 August 2024

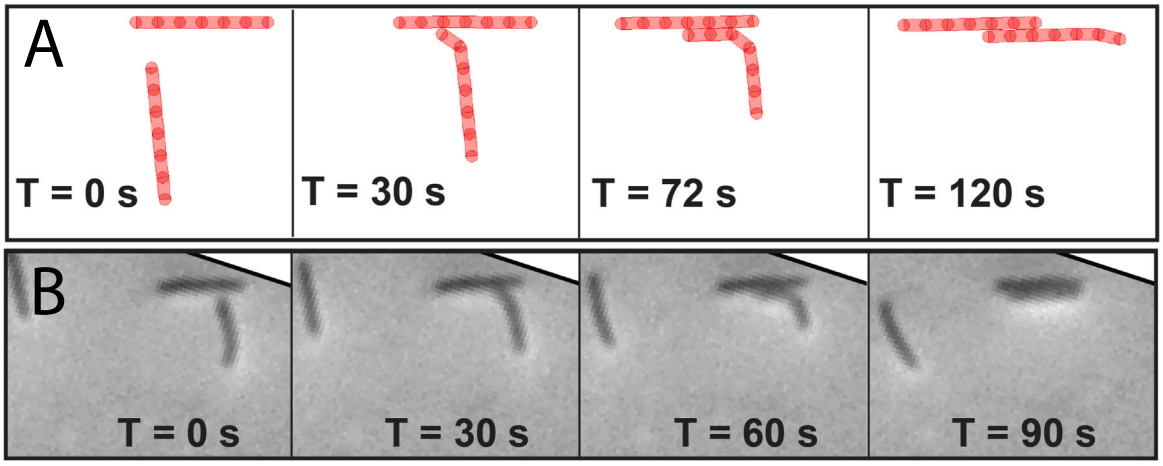

Fig. 1. An example of asymmetric alignment during the collision of two *M. xanthus* cells due to cell–substrate forces. *Source:* Adapted from [6].

tracing rod collisions as they naturally occur and updating the kinetic distribution function accordingly.

A common starting point for such derivations is an application of Boltzmann framework that originated in the kinetic theory of gases. The framework is based on 4 key elements: (i) the geometry (shape) of interacting particles; (ii) the type of interactions, that determines how particle states change in collisions; (iii) the proper asymptotic regime in the model parameters; and (iv) the assumption of "molecular chaos", that is the absence of two-particle correlations. Importantly, the validity of hypothesis (iv) depends on the geometry of interacting particles and the type of interactions.

This modeling approach for self-propelled particles aligning through collisions has been taken up by several authors [14,17,21,23,28–30]. In Bertin et al. (2006) [14], authors consider spherically shaped cells that experience *polar alignment* with some amount of noise in the post-collisional orientations. Their model is based on the zero-order approximation of the interaction operator, which amounts to treating terms of order $\frac{Nl^2}{L^2}$ as negligible, where N represents the number of particles, l denotes the particle size (radius), and L signifies a macroscopic length scale. This approximation signifies an asymptotic regime where variations in the kinetic function across distances comparable to the particle size can be disregarded, reminiscent of the classical Boltzmann equation. Under these conditions and hypothesis (iv), the authors derived a kinetic equation for the distribution of cells and a reduced hydrodynamic-type model for the first few moments of the cell density distribution, assuming that the macroscopic motion is slow.

Cells of more realistic shape (rod-shaped cells) were considered in Hittmeir et al. (2021) [17]. The authors built a kinetic model in which a pair of colliding co-oriented cells (rods with angle difference $|\theta_1 - \theta_2| < \pi/2$) change their orientation to their average alignment; otherwise ($|\theta_1 - \theta_2| > \pi/2$) both colliding cells reverse their direction of motion. This complex interaction consists of a partial *polar alignment* and a partial reversal. Again, the kinetic model is obtained using the zero-order approximation of the interaction operator and the molecular chaos assumption. For special sets of cell orientations, the authors identify the corresponding set of equilibrium distributions and derive a hydrodynamic-type model in the limit $\frac{Nl}{L} \to \infty$.

Over the last decade, the validity of Boltzmann formalism has come into question. Evidence has shown that in some biological systems, this modeling approach is not enough to reproduce the observed system dynamics due to either weak binary interactions when stronger, multi-particle interactions are needed [30], or due to rapid cluster formation that violates the molecular chaos hypothesis [21,28,29]. These latter studies suggest that biologically-relevant phenomena reliant on cluster formation, such as the transitions from unordered to collective motion [18,31,32], may not be accurately modeled with Boltzmann-type equations. However, results from Thüroff et al. (2013) [28] suggest that a Boltzmann approach can be appropriate for systems that align weakly or gradually over time.

In this paper, we present a refined kinetic model that offers a more precise representation of cell interactions, taking into account both the nature of these interactions and the specific asymptotic regime governing the interaction operator. Furthermore, we examine the compatibility between these assumptions and the underlying hypothesis of molecular chaos.

We assume that cells are rod-shaped and when a given cell strikes a second cell, it instantly turns around its "head" (the tip of the rod in the direction of motion) to match a second cell's orientation. Thus, in our model, the re-orientations are truly *nematic* and also *asymmetric*, in agreement with empirical observations of myxobacteria alignment, Fig. 1. For the asymptotic parameter regime, our model goes beyond the zero-order approximation used in the above-mentioned papers, by including the next-order correction. In fact, if one takes the values of model parameters from typical experiments with myxobacteria, one can see that the second-order correction term (in a non-dimensional equation) can be as large as 0.1 and, thus, is not negligible. We derive our main kinetic equation for the nematic alignment under these assumptions (Section 2, Eq. (12)). In Section 3, we reduce this general kinetic equation to a system of numerically tractable PDEs by assuming only a finite number of orientations are present. The system turns out to be conservative and of the hyperbolic type. We then use a Lax–Friedrichs numerical algorithm, specifically designed to treat such systems, to obtain the numerical solutions.

Additionally, in Section 3 we perform a comparative study of the numerical solutions of the PDEs with the agent-based simulations to determine the validity of the molecular chaos assumption. Our main finding here is that, unless an appreciable amount of noise is added to the model, the molecular chaos assumption does not hold. We show that even in simple cases the agent model exhibits cluster formation, with the rate of clustering increasing with the number of cells for the asymptotic regime considered.

As previously discussed, these results do not come as a complete surprise; instead, they validate the criticisms directed towards the Boltzmann framework when applied to scenarios involving self-propelled, rod-shaped cells engaged in asymmetric nematic alignment.

2. Derivation of kinetic equation

Our goal is to derive a tractable kinetic description of a system of N self-propelled rods in of length l moving at constant speed v in 2

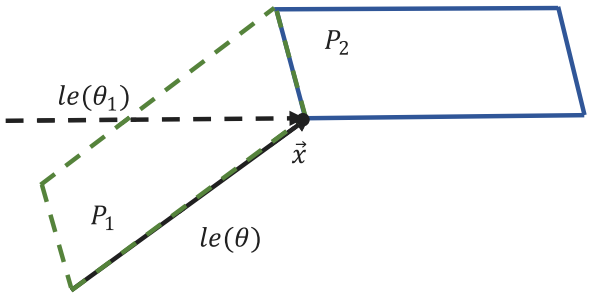

Fig. 2. Geometry of the collision scheme considered in our model. P_1 is the set of heads of rods with orientation θ_1 that will hit the side of the rod with orientation θ having its head at $\mathbf{x}$, at time t, when it moves for Δt units of time. Likewise, a rod with orientation θ at $\mathbf{x}$ at time t will hit the side of a rod with orientation θ_1 having its head in P_2 at time t. P_1 is formed by vectors $l\mathbf{e}(\theta)$ and $v\ \Delta t(\mathbf{e}(\theta_1)-\mathbf{e}(\theta))$. P_2 is formed by vectors $l\mathbf{e}(\theta_1)$ and $v\ \Delta t(\mathbf{e}(\theta_1)-\mathbf{e}(\theta))$.

dimensions, starting from a microscopic description of collisions. Let $f(\mathbf{x},\theta,t)$ be the probability a rod with orientation θ has its head located at $\mathbf{x}\in\Omega=[0,L]\times[0,L]$ at time t. We will next derive a kinetic equation for f by finding an expression for the change in f over a single time step of size Δt. To this end, we make several assumptions about rod collisions. First, we assume that collisions are binary events, with the striking rod reorienting to match the struck rod's orientation modulo π. This results in the nematic alignment of rods. Motivated by *M. xanthus* dynamics, we further assume that reorientation occurs through the head of the rod. Since we assume binary collisions, we will make use of the 2-particle distribution function $f_2(\mathbf{x},\theta,\mathbf{x}_1,\theta_1,t)$ to help calculate collision events.

Denote by Δf the change of f along the trajectory:

$$\Delta f(\mathbf{x},\theta,t)=f(\mathbf{x}+v\mathbf{e}(\theta)\ \Delta t,\theta,t+\Delta t)-f(\mathbf{x},\theta,t),$$

with $N\Delta f$ representing the change in the number of rods with a given location and orientation. In the absence of collisions, the change is zero. If a collision occurred it could result in the gain or loss of rods of orientation θ. The associated geometry of rods for gain and loss is determined by fixing a spatial location $\mathbf{x}$ and considering two cases using two (non-interacting) rods with orientations θ and θ_1 and heads at $\mathbf{x}$. We then look at the sets of collisions in the next dt time that will result in either a gain of a rod with orientation θ (due to a collision with a θ-rod) or an equivalent loss (due to the θ-rod colliding). This yields two regions $P_1(\mathbf{x},\theta,\theta_1)$ and $P_2(\mathbf{x},\theta,\theta_1)$ where another rod could be located to cause a collision (see Fig. 2).

We can now use this setup to derive the change Δf.

$$\begin{aligned}\Delta f(\mathbf{x},\theta,t)=&-(N-1)\int_{-\pi}^{\pi}\int_{P_2(\mathbf{x},\theta,\theta_1)}f_2(\mathbf{x},\theta,\mathbf{x}_1,\theta_1,t)\,d\mathbf{x}_1d\theta_1\\&+(N-1)\int_{\theta-\pi/2}^{\theta+\pi/2}\int_{P_1(\mathbf{x},\theta,\theta_1)}f_2(\mathbf{x},\theta_1,\mathbf{x}_1,\theta,t)\,d\mathbf{x}_1d\theta_1\\&+(N-1)\int_{\theta-\pi/2}^{\theta+\pi/2}\int_{P_1(\mathbf{x},\theta+\pi,\theta_1)}f_2(\mathbf{x},\theta_1,\mathbf{x}_1,\theta+\pi,t)\,d\mathbf{x}_1d\theta_1\end{aligned}\tag{1}$$

To get a closed-form equation for f we employ a commonly used assumption that 2-particle distribution $f_2(\mathbf{x},\theta,\mathbf{x}_1,\theta_1,t)$ can be written as the product of the marginal distributions $f(\mathbf{x},\theta,t)$ and $f(\mathbf{x}_1,\theta_1,t)$, i.e.

$$f_2(\mathbf{x},\theta,\mathbf{x}_1,\theta_1,t)=f(\mathbf{x},\theta,t)f(\mathbf{x}_1,\theta_1,t),\tag{2}$$

for all pairs $(\mathbf{x},\theta)$ and $(\mathbf{x}_1,\theta_1)$. This first-order moment closure is known as statistical independence, or molecular chaos, as it implies that the presence of one rod does not affect the probability of finding the other at the given position and orientation. Next, we write the integral terms using a Taylor expansion in $\mathbf{x}_1$

$$f(\mathbf{x}_1,\theta_1,t)=f(\mathbf{x},\theta_1,t)+\nabla_{\mathbf{x}}f(\mathbf{x},\theta_1,t)\cdot(\mathbf{x}_1-\mathbf{x})+O(|\mathbf{x}_1-\mathbf{x}|^2),\tag{3}$$

so that only an integral over θ_1 remains. Note that $|\mathbf{x}_1-\mathbf{x}|=O(l)$ since two rods must be close to enable collision. A geometric computation shows that the regions P_1 and P_2 where collisions can take place have area $|P_1|=|P_2|=lv\ \Delta t|\sin(\theta-\theta_1)|$. Substituting the Taylor expansion into the expression for Δf and using the areas of P_1, P_2 with the integrals

$$\int_{P_2(\mathbf{x},\theta,\theta_1)}(\mathbf{x}_1-\mathbf{x})\,d\mathbf{x}_1=\frac{l^2v\ \Delta t}{2}|\sin(\theta-\theta_1)|\,\mathbf{e}(\theta_1)+O(l^3v\ \Delta t),\tag{4}$$

and

$$\int_{P_1(\mathbf{x},\theta,\theta_1)}(\mathbf{x}_1-\mathbf{x})\,d\mathbf{x}_1=\frac{l^2v\ \Delta t}{2}|\sin(\theta-\theta_1)|\,\mathbf{e}(\theta)+O(l^3v\ \Delta t),\tag{5}$$

we obtain

$$\begin{aligned}\Delta f(\mathbf{x},\theta,t)=&(N-1)lv\ \Delta t\int_{\theta-\pi/2}^{\theta+\pi/2}|\sin(\theta-\theta_1)|f(\mathbf{x},\theta+\pi,t)f(\mathbf{x},\theta_1,t)\,d\theta_1\\&-(N-1)lv\ \Delta t\int_{\theta-\pi/2}^{\theta+\pi/2}|\sin(\theta-\theta_1)|f(\mathbf{x},\theta,t)f(\mathbf{x},\theta_1+\pi,t)\,d\theta_1\\&+\frac{(N-1)l^2v\ \Delta t}{2}\int_{\theta-\pi/2}^{\theta+\pi/2}|\sin(\theta-\theta_1)|f(\mathbf{x},\theta_1,t)\left(\mathbf{e}(\theta)\cdot\nabla_{\mathbf{x}}f(\mathbf{x},\theta,t)+\mathbf{e}(\theta+\pi)\right.\\&\left.\cdot\nabla_{\mathbf{x}}f(\mathbf{x},\theta+\pi,t)\right)d\theta_1\\&-\frac{(N-1)l^2v\ \Delta t}{2}\int_{\theta-\pi/2}^{\theta+\pi/2}|\sin(\theta-\theta_1)|f(\mathbf{x},\theta,t)\left(\mathbf{e}(\theta_1)\cdot\nabla_{\mathbf{x}}f(\mathbf{x},\theta_1,t)\right.\\&\left.+\mathbf{e}(\theta_1+\pi)\cdot\nabla_{\mathbf{x}}f(\mathbf{x},\theta_1+\pi,t)\right)d\theta_1\\&+O(Nl^3v\ \Delta t\max|f|\max|\nabla_{\mathbf{x}}^2f|)+O(Nl^2\ \Delta t^2).\end{aligned}\tag{6}$$

Dividing the equation above by Δt and letting $\Delta t\to 0$, we obtain the kinetic equation

$$\partial_t f+v\mathbf{e}(\theta)\cdot\nabla_{\mathbf{x}}f=(N-1)lvQ_0+\frac{(N-1)l^2v}{2}Q_1+O\left(Nl^3v\max|f|\max|\nabla_{\mathbf{x}}^2f|\right),\tag{7}$$

where

$$Q_0=\int_{\theta-\pi/2}^{\theta+\pi/2}|\sin(\theta-\theta_1)|\left(f(\mathbf{x},\theta+\pi,t)f(\mathbf{x},\theta_1,t)-f(\mathbf{x},\theta,t)f(\mathbf{x},\theta_1+\pi,t)\right)d\theta_1,\tag{8}$$

and

$$\begin{aligned}Q_1=&\int_{\theta-\pi/2}^{\theta+\pi/2}|\sin(\theta-\theta_1)|f(\mathbf{x},\theta_1,t)\mathbf{e}(\theta)\cdot\nabla_{\mathbf{x}}\left(f(\mathbf{x},\theta,t)-f(\mathbf{x},\theta+\pi,t)\right)d\theta_1\\&-\int_{\theta-\pi/2}^{\theta+\pi/2}|\sin(\theta-\theta_1)|f(\mathbf{x},\theta,t)\mathbf{e}(\theta_1)\cdot\nabla_{\mathbf{x}}(f(\mathbf{x},\theta_1,t)-f(\mathbf{x},\theta_1+\pi))\,d\theta_1.\end{aligned}\tag{9}$$

In deriving the Q_1 term we used the identity $\mathbf{e}(\theta+\pi)=-\mathbf{e}(\theta)$.

We nondimensionalize Eq. (7) by setting $\tau=L/v$ and rescaling the variables using

$$\hat{\mathbf{x}}=\mathbf{x}/L,\quad \hat{t}=t/\tau,\quad \hat{f}(\hat{\mathbf{x}},\theta,\hat{t})=L^2f(\hat{\mathbf{x}}L,\theta,\hat{t}\tau).\tag{10}$$

Dropping hats, the resulting scaled kinetic equation is

$$\partial_t f+\mathbf{e}(\theta)\cdot\nabla_{\mathbf{x}}f=\frac{(N-1)l}{L}Q_0+\frac{(N-1)l^2}{2L^2}Q_1+O\left(\frac{Nl^3}{L^3}\right),\tag{11}$$

where we assumed that the variations in the kinetic density f are bounded, that is $\max|f|\max|\nabla_{\mathbf{x}}^2f|\le C$. For a typical experiment with $N=1000$ *M. xanthus* bacteria ($l=5$ μm) on a domain of size $L=10^3$ μm, we have parameter values $\frac{Nl}{L}=5$, $\frac{Nl^2}{L^2}=0.025$, and $\frac{Nl^3}{L^3}=0.000125$. Thus, when C is of order 1, a reasonable approximation is keeping only the first two terms on the right-hand side. We set $\kappa=\frac{Nl^2}{2L^2}$. The parameter κ is related to the mean free path d and rod length l by

$$\kappa\le\frac{l}{2d}.$$

See (A.1) of the Appendix for details. The binary collision assumption fails if d is of order l or smaller, meaning that κ should be small. In the numerical simulations in the subsequent sections, we will restrict $\kappa < 0.5$. The resulting kinetic equation becomes

$$\partial_t f + \mathbf{e}(\theta)\cdot\nabla_{\mathbf{x}} f = \frac{2\kappa L}{l} Q_0(f) + \kappa Q_1(f). \tag{12}$$

In the model of alignment that we consider in this paper, a rod after an interaction assumes the orientation of the rod it collides with. The set of orientations θ_i, $\theta_i + \pi$, $i = 1,\dots,k$, if present initially, will be preserved by the dynamics of transport and collision. In such situations, the kinetic density f is determined by the set of $2k$ densities of the corresponding orientations, and Eq. (12) can be written as a system of $2k$ partial differential equations for the orientation densities. An example of such a system is considered in the following sections.

3. Numerical solutions and results from agent-based simulations for case study

In the absence of correlations in the underlying system, kinetic equations derived from Boltzmann's hypothesis should accurately model the system's evolution in time. However, the presence of correlations can cause discrepancies to appear. Here we will test the accuracy of our kinetic equation by comparing the behavior of numerical solutions to agent-based simulations of the underlying system. We will use a test case to demonstrate that even for simple setups, the microscopic rules of collision lead to a buildup of orientational correlations, causing the correlation-free model to underestimate the effects of rod-rod interactions. While this test case does not capture the complexity present in many physical systems, it is enough to demonstrate the need to account for correlations between rods when modeling active matter systems such as bacterial communities.

3.1. A model with two orientations

Consider Eq. (12) for distributions with n fixed orientations $f(\mathbf{x},\theta,t) = \sum_{i=1}^{n} \rho_i(\mathbf{x},t)\delta(\theta-\theta_i)$, $\mathbf{x} = [x,y]^T$. This substitution will result in a system of n PDEs in two spatial dimensions. This system is typically non-conservative, making it more difficult to solve numerically over long periods of time. To illustrate our point about the growth of correlations, we will focus on a reduced case with two orientation angles θ_1 and θ_2 where $|\theta_2 - \theta_1| \le \pi/2$. Then there is no nematic alignment and, thus, the term $Q_0(f)$ vanishes. Additionally, as we will show, the system of two PDEs can be written in a conservative form under certain assumptions about the initial distribution of orientations. This makes accurate numerical solutions easier to obtain. Substituting $f(\mathbf{x},\theta,t) = \rho_1(\mathbf{x},t)\delta(\theta-\theta_1) + \rho_2(\mathbf{x},t)\delta(\theta-\theta_2)$ into (12) yields a system for $\boldsymbol{\rho} = (\rho_1,\rho_2)$ of the form

$$\partial_t \boldsymbol{\rho} + A(\boldsymbol{\rho})\partial_x \boldsymbol{\rho} + B(\boldsymbol{\rho})\partial_y \boldsymbol{\rho} = 0 \tag{13}$$

where the matrices A and B are given by

$$A = \begin{bmatrix} \cos(\theta_1) + \kappa|\sin(\theta_2-\theta_1)|\cos(\theta_2)\rho_2 & -\kappa|\sin(\theta_2-\theta_1)|\cos(\theta_1)\rho_1 \\ -\kappa|\sin(\theta_2-\theta_1)|\cos(\theta_2)\rho_2 & \cos(\theta_2) + \kappa|\sin(\theta_2-\theta_1)|\cos(\theta_1)\rho_1 \end{bmatrix},$$

$$B = \begin{bmatrix} \sin(\theta_1) + \kappa|\sin(\theta_2-\theta_1)|\sin(\theta_2)\rho_2 & -\kappa|\sin(\theta_2-\theta_1)|\sin(\theta_1)\rho_1 \\ -\kappa|\sin(\theta_2-\theta_1)|\sin(\theta_2)\rho_2 & \sin(\theta_2) + \kappa|\sin(\theta_2-\theta_1)|\sin(\theta_1)\rho_1 \end{bmatrix}.$$

To simplify these kinetic equations to a form easily analyzed, we make two assumptions: that all densities vary only in the spatial direction x so the problem is effectively 1D with $\rho(\mathbf{x},t) = \rho(x,t)$, and that $\theta_1 = \frac{\pi}{4}$, $\theta_2 = \frac{3\pi}{4}$ so the system can be put into conservation form. In this setting, the system (13) is simply

$$\begin{aligned} \partial_t \rho_1 + \frac{\sqrt{2}}{2}\partial_x\left(\rho_1\left[1-\kappa\rho_2\right]\right) &= 0 \\ \partial_t \rho_2 - \frac{\sqrt{2}}{2}\partial_x\left(\rho_2\left[1-\kappa\rho_1\right]\right) &= 0. \end{aligned} \tag{14}$$

We restrict our analysis to the regime $0 < \kappa < 0.5$ to enforce the mean free path of rods is greater than the rod length l (see Appendix A). We will consider a test case with two opposing waves of rods over a constant background density. Each wave is a Gaussian moving over a uniform background density of rods. The initial conditions for ρ_1 and ρ_2 are of the form

$$\rho_i(x,0) = a_i + \frac{b_i}{\sqrt{2\pi}\sigma_i} e^{-(x-c_i)^2/(2\sigma_i^2)} \tag{15}$$

with the constraints $\int_0^1\int_0^1 \rho_1(x,0) + \rho_2(x,0)dxdy = 1$ from conservation and an enforced constraint $a_i/b_i = r_i$ for the ratio of background cells to the cells forming the waves. The final parameters c_i and σ_i then control the location and width of the waves. Additionally, the maximum amplitude $a_i + b_i/(\sqrt{2\pi}\sigma_i)$ set below the bound established in Appendix B. As time evolves, the linear factor $1-\kappa\rho_i$ inside the spatial derivative will decrease both the left-and right-moving waves' speeds when they interact. Finally, we set $c_1 = 0.25$, $c_2 = 0.75$, $\sigma_1 = \sigma_2 = 0.0625$, and $r_i = 7$ so the two waves' peaks will move towards each other and meet at $x = 0.5$. We numerically solve the system (14) using the method described in Appendix C.

3.2. Agent-based model setup

For the agent-based model, we set the domain size to $L = 400$, the velocity to $v = \sqrt{2}$. Each rod $i = 1,\dots,N$ followed the equations of motion

$$\begin{aligned} \frac{d\mathbf{x}_i}{dt} &= v[\cos(\theta_i),\ \sin(\theta_i)]^T \\ \frac{d\theta_i}{dt} &= (\theta_k - \theta_i)\delta(t - T_{i,k}). \end{aligned} \tag{16}$$

where $\delta(t)$ is the Delta distribution and $T_{i,k}$ denotes the times when the ith rod collides with another rod k and reorients. The x-coordinate of the initial location of each rod was determined through random sampling of the initial density profiles $\rho_i(x,0)$ defined in Eq. (15). The y-coordinates were drawn from a uniform distribution $U(0,L)$ to match the assumption in the simplified PDE model (14). Collisions between rods were determined by in a manner consistent with the schematic in Fig. 2 as follows.

The path traveled by rod i was parameterized by $\Gamma_i(s) = \mathbf{x}_i(t) + sv\mathbf{e}(\theta_i)$. Two non-parallel paths intersect when $\Gamma_i(s_1) = \Gamma_k(s_2)$, where $s_1 = (\mathbf{x}_k(t) - \mathbf{x}_i(t))\cdot\mathbf{e}(\theta_k + \pi/2)$ and $s_2 = (\mathbf{x}_i(t) - \mathbf{x}_k(t))\cdot\mathbf{e}(\theta_i + \pi/2)$. This intersection corresponds to rod i colliding with rod k if

1. $0 \le s_1 \le \Delta t$ (the collision happens in Δt time)
2. $s_2 < s_1$ (rod k arrives first)
3. $\|\Gamma_k(s_1) - \Gamma_i(s_1)\| \le l$ (the tail of rod k has not passed the point where the paths cross).

If a collision is detected, rod i undergoes a reorientation to angle θ_k at time $t+\Delta t/2$. While this is an approximation to the actual collision time, it can be made rigorous by restricted the mean-free path of rods to be greater than the rod length l so that $t + \Delta t/2$ is the average collision time. This has a physical argument based on the physical timescale of reorientation l/v (see Appendix A). We confirmed this approximation was valid by comparing it with simulations where a reorientation occurred exactly at time s_1 and found no significant difference in the density distributions produced by the simulations. We also enforced collisions were binary by enforcing that a rod that would collide with multiple rods in a single time step only reoriented once upon the first collision. Lastly, we used the mean free path restriction to take time steps of $\Delta t = l/v$ in the simulation, reducing computational time.

The simulations are deterministic after initial rod positions are sampled, so we combined 1000 simulations to smooth fluctuations and recover the mean behavior. It is worth noting that the systems (13) and (14) describe the evolution of the underlying ensemble average. Each realization of the agent-based model is a single member of the

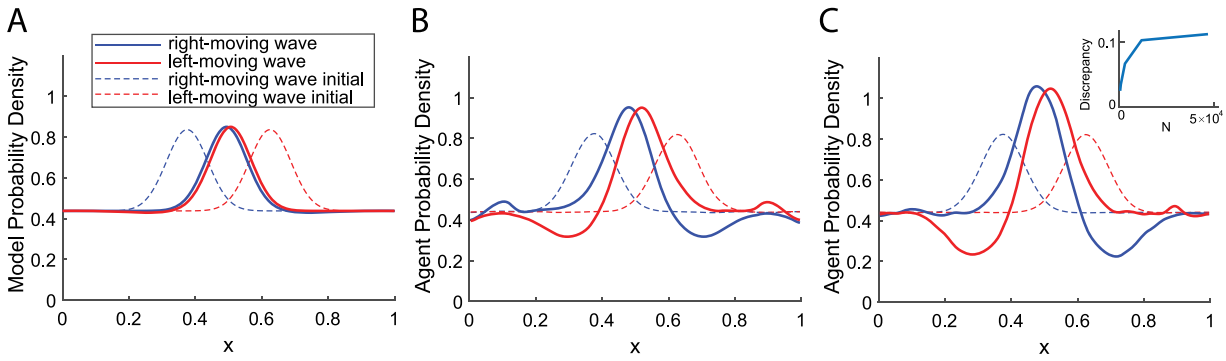

Fig. 3. (A) Numerical solution of the kinetic equations for $\kappa = 0.1$. (B) Density profile for agent-based simulations for $\kappa = 0.1$ with $N = 2856$ rods. (C) Density profile for agent-based simulations for $\kappa = 0.1$ with $N = 45700$ rods. (Inset) The discrepancy at the final time between the kinetic model density profile and the density profile from agent simulations for various numbers of rods. The results indicate that the agent simulations show much greater changes in the density profile and do not converge to the kinetic model in the limit $N \to \infty$, $l \to 0$.

ensemble, so to reasonably compare the agent simulations to the analytical system, we must average over different realizations. While an individual realization does not necessarily have a uniform distribution in the y-direction (and in fact does not usually have a profile in the x-direction that closely matches the analytic solution), after performing this averaging, the agent density profile in the y-direction closely resembles a uniform distribution as measured via the Kolmogorov–Smirnov test and Kullback–Leibler divergence (see Appendix D for details). Since the solutions of system (14) vary spatially only in the x-direction, we compared them to agent-based simulations by looking only at the x-coordinates of simulated rods. We then constructed a 1D kernel density estimate (KDE) using these values. The resulting density profiles were then scaled to probability densities on $x \in [0, 1]$ so they could be compared to the density profiles obtained from numerically solving the kinetic equations.

3.3. Discrepancy between agent-based model and kinetic equations due to cluster formation

Our agent-based simulations deviate from the numerical solutions of the kinetic equations, with the latter exhibiting a far less pronounced change in the density profile shape (Fig. 3 A&B). The peaks of the density profiles for both orientations slow down slightly as they approach each other, but the slowdown and the increase in the peak density are much greater in the agent framework. If this discrepancy is due to not being near the limit $N \to \infty$, $l \to 0$ with κ held constant, increasing the number of simulated rods while keeping $\kappa \propto Nl^2$ fixed should theoretically improve the agreement. However, we see that this is not the case (Fig. 3C). The simulations using higher numbers of rods showed greater discrepancies. This suggests the disagreement is due to one or more flaws in the assumptions used to derive the kinetic equations.

The key assumption used in deriving the Boltzmann-type equation was the statistical independence of the joint probability distribution (2). This allowed us to express the probability that a pair of rods would have a spatial configuration leading to a collision in terms of the probability of each rod individually occupying the corresponding spatial region. This assumption is invalid if there are correlations between rods. Such correlations appear in clusters of aligned rods since they have a high chance of having similar orientations due to collisions. Our collision scheme results in both rods possessing the same orientation, so cluster formation is possible and would be a violation of our assumption of statistical independence.

For our purposes a cluster of rods was defined as a group of k cells at spatial locations $\mathbf{x}_1, \ldots, \mathbf{x}_k$ with $\min_{j \neq i} \|\mathbf{x}_i - \mathbf{x}_j\| \leq \epsilon$ for all $1 \leq i \leq k$. To measure the clustering present in our agent simulations, we used MATLAB's `dbscan` algorithm to group rods. The minimum distance between the heads of rods was picked to be $\epsilon = l/2 + v\Delta t = \frac{3}{2}l$. This value provided a reasonable upper bound that would capture groups of rods that were co-aligned due to collisions. We then measured the proportion of rods in clusters of size $k \geq 4$ (Fig. 4A). As expected, clusters grew over time in our agent simulations, with the rate of growth increasing with κ for fixed N. This increase in κ corresponds to a greater rod length, increasing the chance of collisions between rods.

3.4. Quantifying loss of statistical independence

Since cluster formation is linked to a loss of statistical independence [21,28,29], we next quantified the extent of this loss. Observing a rod with orientation θ_1 would decrease the probability of a nearby rod having orientation θ_2. This is typically captured using two-particle or higher correlation functions. If the system is spatially homogeneous or can be approximated as such, then there are several ingenious ways to calculate these quantities [33–35]. Such an approach is commonly used to analyze systems near the onset of polar or nematic order. In our case, we are far from spatial homogeneity, so we use a different approach.

In our work, we directly calculated metrics from agent simulation data related to the quantity $f_2(x_1, \theta_1, x_2, \theta_2, t) - f(x_1, \theta_1, t) f(x_2, \theta_2, t)$ to see if a loss of independence is present. We first divided our domain $\Omega = [0, L] \times [0, L]$ into 2^{2m} square subregions Ω_{ij}, $i, j = 1, \ldots, 2^m$ with side length $L/2^m$. Since subregions should be large enough to contain small clusters of rods, we set $m = 5$ so that $L/2^m = 12.5$. We pooled all rods appearing in Ω_{ij} across 1000 simulations with different initial agent locations $\mathbf{x}_i(0)$. Then we calculated coarse-grained approximations of the joint and marginal distributions conditioned on rods being in Ω_{ij}

$$\begin{aligned} f_2^{ij}(\theta_1, \theta_2, t) &= \frac{\#\text{ pairs of rods with orientations } (\theta_1, \theta_2) \text{ in box } ij}{\#\text{ pairs of rods in box } ij} \\ f^{ij}(\theta_1, t) &= \frac{\#\text{rods with orientation } \theta_1 \text{ in box } ij}{\#\text{rods in box } ij} \\ f^{ij}(\theta_2, t) &= \frac{\#\text{ rods with orientation } \theta_2 \text{ in box } ij}{\#\text{ rods in box } ij} \end{aligned} \quad . \tag{17}$$

To measure the loss of statistical independence based on orientations in Ω_{ij} at time t, we chose Pearson's correlation coefficient calculated from the estimates of the conditional joint and marginal

$$r^{ij}_{\theta_1\theta_2}(t) = \frac{\left(\sum_{m,n=1,2} \theta_n \theta_m f_2^{ij}(\theta_n, \theta_m, t)\right) - M^2}{\sum_{n=1,2} (\theta_n - M)^2 f^{ij}(\theta_n, t)} \tag{18}$$

where M the mean orientation calculated from $f^{ij}(\theta_1, t)$ and $f^{ij}(\theta_2, t)$. Averaging over all subregions then gives us an average correlation $r_{\theta_1\theta_2}$.

As shown in Fig. 4B, the metric $r_{\theta_1\theta_2}(t)$ shows similar trends over time to the cluster formation. The loss of statistical independence increases over time, with higher values of κ showing a greater loss

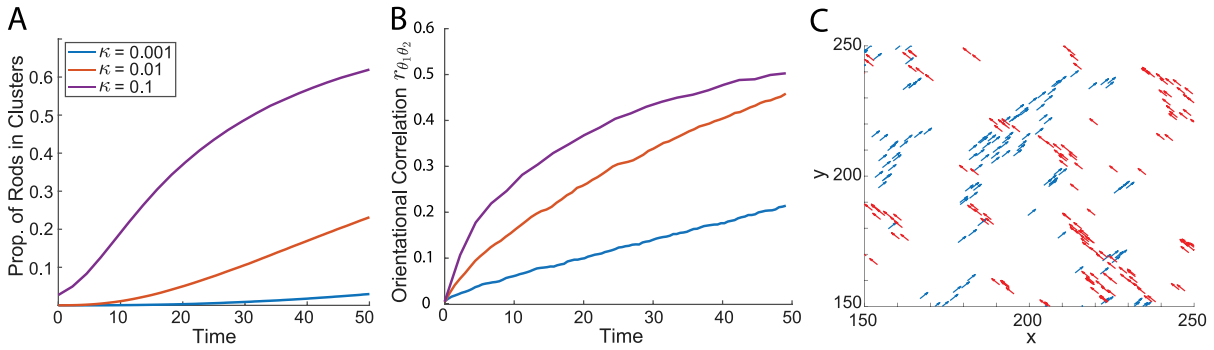

Fig. 4. (A) The percentage of rods in clusters with more than 4 rods over time. This quantity grows over time as rods collide and co-orient. (B) The loss of statistical independence measured via a local orientation correlation coefficient $r_{\theta_1\theta_2}(t)$. Here, the correlations growing over time indicate that it becomes rarer to see nearby rods having different orientations, e.g. cluster formation. (C) Snapshots of an agent simulation at the end of a simulation. The snapshot is taken at the center of the domain where the two waves interact.

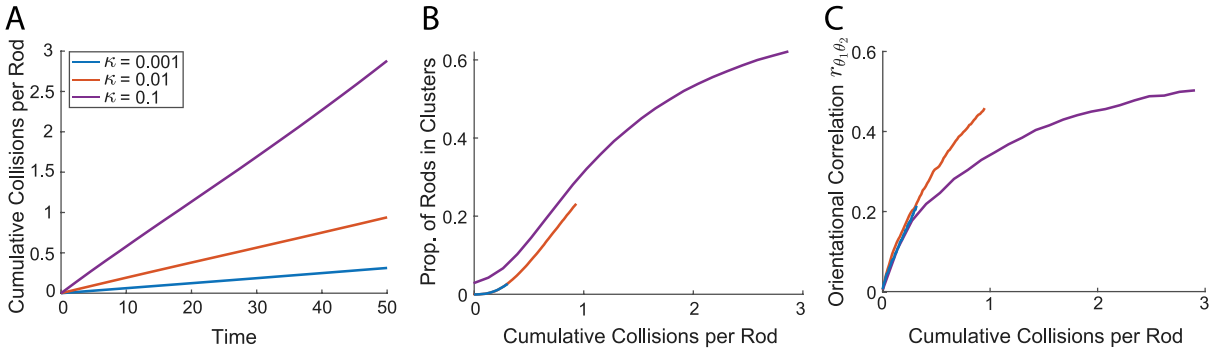

Fig. 5. (A) The total number of collisions experienced on average per rod over time for $\kappa = 0.001$ (blue), $\kappa = 0.01$ (orange), and $\kappa = 0.1$ (purple). (B) The fraction of rods in clusters with more than 4 rods versus the mean number of collisions experienced per rod by time t. This is plotted for $\kappa = 0.001$ (blue), $\kappa = 0.01$ (orange), and $\kappa = 0.1$ (purple) (C) The orientational correlation coefficient $r_{\theta_1\theta_2}(t)$ between nearby pairs of rods versus the mean number of collisions experienced per rod by time t. Both figures show some data collapse when compared to Fig. 3, especially for low mean rod collisions per rod.

for fixed N. This reflects the fact that the chance of finding a pair of rods close together with different orientations is lowered from what is expected if statistical independence holds.

Since cluster formation results from the co-alignment between rods upon collision, it is natural to see if the increase in cluster growth with higher values of κ is due to a greater number of collisions. Calculating the mean number of collisions per rod by time t shows that the number does increase as κ increases (Fig. 5A). Furthermore, there is strong evidence of data collapse when plotting both the proportion of rods in clusters (Fig. 5B) and the loss of statistical independence versus the cumulative number of collisions per rod (Fig. 5C). There is a slight difference in the rescaled curve for $\kappa = 0.1$ compared to the other two curves. This results from some rods starting in clusters at $t = 0$ at higher densities. The reasons for the deviation in the rescaled $r_{\theta_1\theta_2}$ cure for $\kappa = 0.1$ is less clear but could result from cluster–cluster interactions once most rods reside in such clusters. The rescaling is based on rod–rod collisions, so cluster–cluster interactions might not fully be accounted for.

3.5. Improving agreement between agent simulations and kinetic equations by inhibiting cluster formation

While the results of our simulations have indicated close links between cluster formation, loss of independence, and the discrepancy between the equations and agent simulations, they have not shown a strict cause and effect. To illustrate that clustering is the main cause of the discrepancy, we introduce diffusion in y-direction into our agent simulations. The addition of this noise will cause rods forming a cluster to slowly drift apart at a rate dependent on the noise strength. This addition will not impact the test case we considered for the kinetic model. Since initial conditions are constant in the y-direction, the system given in (14) will remain unchanged by the vertical diffusion.

We implemented the same sets of agent simulations as before ($N = 2856$, $\kappa = 0.1$) with the addition of different levels of noise σ. Agent rods step in the y-direction a random distance drawn from a normal distribution $N(0, \sigma)$ every $\Delta t = l/v$. Since agent simulations are run with unscaled variables, we nondimensionalize the noise by using the scaling $\sigma \to \sigma/(l/\sqrt{2})$ in order to compare the strength of the noise to the rod length l. The results of these simulations show that the addition of noise in the y-direction improves agreement between the agent simulations and the kinetic equations, with the former now resembling the latter for a sufficient level of noise (Fig. 6A). Increasing the noise strength from zero reduces the measured discrepancy between the kinetic and agent density profiles (Fig. 6B) and decreases the proportion of rods in clusters (Fig. 6C). However, the discrepancy is reduced only up to a point. Once the strength of the scaled noise exceeds roughly 1 (corresponding to the standard deviation of the normal distribution equaling the projection of a rod in the y-direction), the discrepancy increases slightly before plateauing. A close analysis of the simulation average showed that this discrepancy results from rods in the uniform background being added to the leading front of a wave by rods in the opposing wave (Movie 1). Why this is the case is unclear; however, the reduction in clustering slows down at around the same level of noise. It is possible that there are some aspects of rod correlations that the added diffusion does not affect. For example, our collision scheme results in both rods having similar x-coordinates. The addition of vertical diffusion does not change this either. Therefore, successive collisions result

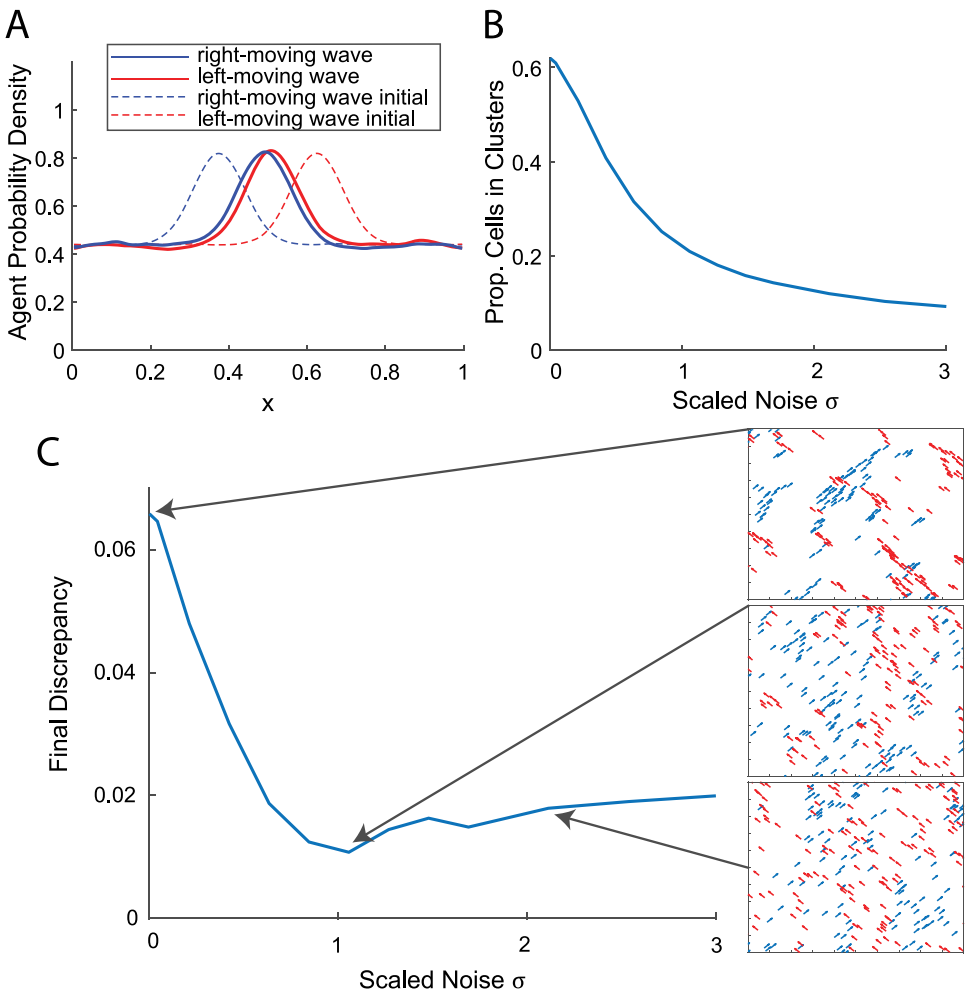

Fig. 6. (A) Density profile for agent-based simulations with y-directional scaled noise of 1.06 for $\kappa = 0.1$ with $N = 2856$ rods. A scaled noise level of 1 corresponds to an agent rod's vertical movement over time $\Delta t = l/v$ being distributed normally as $y(t+dt) - y(t) \sim N(l\sin(\theta_i), l\sin(\theta_i)) = N(l/\sqrt{2}, l/\sqrt{2})$ in between collisions, or equivalently to a vertical diffusion coefficient of $l^2/4$. (B) Percentage of rods in clusters with more than 4 rods versus noise in y-direction. Increasing the noise in the vertical direction decreases the proportion of rods in larger clusters (C) Discrepancy between the kinetic model and the agent-based simulations for different levels of white noise in the y-direction. The discrepancy initially drops sharply but then increases slightly once the strength of the noise increases past 1, the length of a rod projected in the y-direction. Snapshots of agent simulations near noise levels of 0, 1, and 2 are shown on the right. The snapshots are taken at the final time in the center of the domain ($[150, 250] \times [150, 250]$) where the two waves interact.

in more rods sharing similar x-coordinates, and potentially forming vertical bands of rods regardless of vertical diffusion.

4. Discussion

In this paper, we developed a kinetic model for the alignment of self-propelled hard rods where collisions result in asymmetric alignment. Using this model, we showed Boltzmann formalism severely underestimates the change in rod density profiles when two opposing waves of rods interact. We explicitly measured the loss of statistical independence that invalidates the classic assumption of molecular chaos Boltzmann-type equations rely on. Such a loss corresponds to the formation of rod clusters due to alignment from binary rod collisions. Our results mirror those in other studies [21,28], however, we have built upon these works by showing that mechanisms that destroy or inhibit cluster formation help restore agreement between the kinetic model and agent-based implementations of the microscopic alignment rules. As this discrepancy occurs even in the simple setup we consider, our work highlights the need to extend current methodologies beyond Boltzmann-type kinetic equations in order to accurately capture the properties of active matter in biological systems.

Boltzmann's hypothesis can be justified when the mean free path is large compared to the range of local interactions, however, this is rarely satisfied at realistic densities when ordered motion is established [36]. Additionally, several studies have indicated that rapid cluster formation can lead to a strong violation of the molecular chaos assumption needed in the Boltzmann approach [21,28]. While gradual alignment results in a better match, in principle any collision rule between particles resulting in alignment can cause correlations to appear. Such collisions are prevalent in collective dynamics at the cellular level due to a low Reynolds number, where cells must actively exert energy to maintain their motion. This is in contrast to Boltzmann gas dynamics, where collisions are assumed to be non-elastic and conserve momentum, resulting in particles simply bouncing off each other. In addition to violations of Boltzmann's hypothesis, the assumption of binary interactions used in such models is not enough to reproduce the observed dynamics in some biological systems [30]. Binary interactions can simply be too weak to produce the alignment seen experimentally, even when corrections are made to account phenomenologically for correlations. These breakdowns of Boltzmann-type models suggest they are an overly-simplistic approach to modeling the emergence or stability of collective alignment. The emergence of local order almost by definition involves the breakdown of statistical independence and the growth of correlations as agents align and start moving together, violating Boltzmann's hypothesis.

There are several ways to extend kinetic models to incorporate orientational correlations. Perhaps the simplest is to explicitly extend the kinetic model to explicitly include equations for clusters of various sizes. Gain and loss terms for these additional equations are then the natural result of collisions among clusters and rods [37,38]. Peruani et al. (2010) developed a framework where cluster size was explicitly tracked in a hierarchy of equations, while Weber et al. (2013) [38] considered a simplified framework with two reaction equations for clusters and single cells. Another set of approaches for incorporating correlations involves direct modifications to the moment closure method. A simple example is replacing the joint distribution $f_2(x_1,\theta_1,x_2,\theta_2,t)$ with $\chi(\theta_2-\theta_1)f(x_1,\theta_1,t)f(x_2,\theta_2,t)$, where $\chi(\theta_2-\theta_1)$ is a phenomenological term accounting for correlations between different angles [30]. More sophisticated methods involve higher-order moment closures of the BBGKY hierarchy [6,39,40] using the so-called cluster expansion that explicitly incorporates the evolution of the joint distribution f_2 [41]. Such an approach was used by Chou and Ihle for Vicsek-style models to extend beyond mean-field theory [42]. With the rapid advancement of biological studies in the last decades, developing and applying new analytical models to understand active matter in biology is of crucial importance. Creating a tractable class of models that can capture correlations or non-binary interactions would provide a cornerstone for this young field.

CRediT authorship contribution statement

Patrick Murphy: Writing – review & editing, Writing – original draft, Software, Formal analysis, Conceptualization. **Misha Perepelitsa:** Writing – review & editing, Writing – original draft, Investigation, Formal analysis, Conceptualization. **Ilya Timofeyev:** Writing – review & editing, Writing – original draft, Software, Investigation, Formal analysis. **Matan Lieber-Kotz:** Software, Investigation. **Brandon Islas:** Software, Investigation. **Oleg A. Igoshin:** Writing – review & editing, Writing – original draft, Supervision, Project administration, Investigation, Conceptualization.

Declaration of competing interest

The authors declare that they have no known competing financial interests or personal relationships that could have appeared to influence the work reported in this paper.

Research data availability

The code used to generate the results in this paper is published under a GNU General Public License and can be access at https://github.com/pmurphy12/Boltzmann-breakdown-code.

Acknowledgments

Research is supported by National Science Foundation Division of Mathematical Sciences awards 1903270 (to M.P. and I.T.) and 1903275 (to OAI and PM). This work was supported in part by the Big-Data Private-Cloud Research Cyberinfrastructure MRI-award funded by NSF under grant CNS-1338099 and by Rice University's Center for Research Computing (CRC). We also would like to thank prof. D. Kuzmin (TU Dortmund) for helpful discussions on the numerical methods for the kinetic model presented in this paper.

Appendix A. Mean free path

The mean free path (MFP) is defined as the average distance that a rod moves between collisions. This distance can be computed as the product of the speed v and the time τ a rod moves between reorientations. To estimate τ, we first compute the number of rods with orientation $\mathbf{e}(\theta)=(\cos\theta,\sin\theta)$ that will collide with a given rod (rod 1) in the time $[t^*,t^*+\Delta t]$, were t^* marks the last change in rod 1's orientation. Without loss of generality, we consider rod 1 as moving horizontally to the right, as in Fig. 7. Suppose that a coordinate system is chosen so that the rod is at rest. Then the velocity of rods with orientation θ is described by the vector $\mathbf{w}=v(\cos\theta-1,\sin\theta)$. The heads of the rods that rod 1 can collide with are located in a parallelogram P formed by vectors $\mathbf{w}\,\Delta t$ and $l\mathbf{e}(\theta)$. The area of this parallelogram equals $|\sin\varphi(\theta)|vl\,\Delta t$. Using that $Nf(x,\theta,t^*)$ is the local number of rods with a given orientation, we estimate the number of collisions with θ-oriented rods in time Δt as $vlNf(x,\theta,t^*)|\sin\varphi(\theta)|\,\Delta t$, which is maximized at $\varphi=\pi/2$. Thus, the number of collisions over all orientations in Δt time can be estimated as

$$vlN\,\Delta t\int f(x,\theta,t^*)\,d\theta\le n(x,t^*)vl\,\Delta t,$$

where $n(x,t^*)$ is the local rod number density. From this, we obtain an upper bound for the frequency of collisions as $n(x,t^*)vl$. The time between collisions and the MFP are then bounded by

$$\tau\ge\frac{1}{n(x,t^*)vl},\quad d\ge\frac{1}{n(x,t^*)l}.$$

Note that both τ and the MFP d are local quantities depending on x.

For the model we consider in this paper, we restrict the MFP to $d\ge l$. The rationale behind this is physics-based. When two rods collide, there is a characteristic time scale for reorientation to occur given by $\tau_\theta=l/v$ [7]. Therefore it makes sense to restrict the mean time between collisions τ to the regime $\tau\ge\tau_\theta=l/v$. This naturally yields $d\ge l$.

Our assumption that $d\ge l$ puts a restriction on the local density of the form $n(x,t^*)l^2\le 1$, and subsequently on the parameter κ of the form

$$\kappa=\frac{Nl^2}{2L^2}\le\frac{1}{2}l^2\max_x n(x,t^*)\le\frac{1}{2}. \tag{A.1}$$

Here we use that N/L^2 is a lower bound on the maximum of $n(x,t^*)$. Note that we cannot have $\kappa=0$ without the local density being identically 0.

Appendix B. Domain of hyperbolicity of system of Eqs. (14)

Here we will determine conditions under which system (14) is hyperbolic. The system is given by

$$\begin{aligned}\partial_t\rho_1+\frac{\sqrt{2}}{2}\partial_x\left[\rho_1(1-\kappa\rho_2)\right]&=0\\ \partial_t\rho_2-\frac{\sqrt{2}}{2}\partial_x\left[\rho_2(1-\kappa\rho_1)\right]&=0,\end{aligned} \tag{B.1}$$

where $\kappa=\frac{Nl^2}{2L^2}$. Denote the column vector $U=(\rho_1,\rho_2)^T$ and column of the fluxes $F(U)=\frac{\sqrt{2}}{2}(\rho_1-\kappa\rho_1\rho_2,-\rho_2+\kappa\rho_1\rho_2)^T$. Then the system of equations is expressed as

$$\partial_t U+\partial_x F(U)=0.$$

The system is hyperbolic if the eigenvalues of the gradient matrix

$$\nabla_U F(U)=\frac{\sqrt{2}}{2}\begin{bmatrix}1-\kappa\rho_2 & -\kappa\rho_1\\ \kappa\rho_2 & -1+\kappa\rho_1\end{bmatrix}$$

are real. The eigenvalues equal

$$\lambda_\pm=\frac{1}{2\sqrt{2}}\left(\kappa(\rho_1-\rho_2)\pm\sqrt{\kappa^2(\rho_1-\rho_2)^2+4-4\kappa(\rho_1+\rho_2)}\right).$$

Thus, the system is hyperbolic whenever

$$\kappa^2(\rho_1-\rho_2)^2+4-4\kappa(\rho_1+\rho_2)\ge 0$$

with a sufficient condition

$$\kappa(\rho_1+\rho_2)\le 1.$$

Since (A.1) implies $\kappa<0.5$, our kinetic model (14) must be restricted to cases where the sum of the maximum density profiles for ρ_1 and ρ_2 total less than 2.

Fig. 7. Vector geometry used in the estimation of the MFP. (A) Rod at $\mathbf{x}$ where $\mathbf{e}(\theta) = (\cos\theta, \sin\theta)$ moves with velocity $v\mathbf{e}(\theta)$. In the reference coordinates of a horizontally moving rod with velocity $(v, 0)$, the rod velocity is $\mathbf{w}$. (B) a rod moving horizontally to the right, during time interval $[t^*, t^* + \Delta t]$ can collide with a rod which has orientation $\mathbf{e}(\theta)$ whose center is located in the parallelogram P, formed by vectors $\mathbf{w}\,\Delta t$ and $l\mathbf{e}(\theta)$. The area of the parallelogram equals $|\sin\varphi| v l\ \Delta t$.

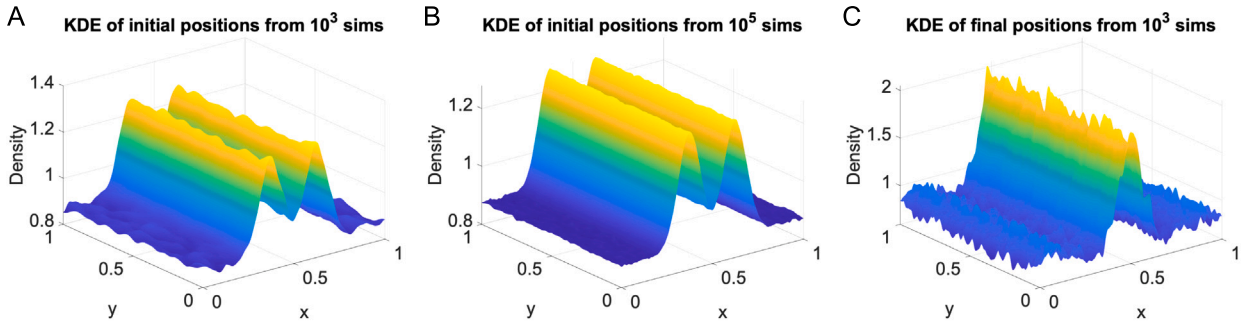

Fig. 8. Kernel density estimates using rods from agent simulations in 2D space. (A) Initial rod positions taken from 1000 simulations. (B) Initial rod positions taken from the equivalent of 10^5 simulations. (C) Final rod positions take from the 1000 simulations used in (A).

Appendix C. Numerical methods

We express the system in (14) in flux form

$$\partial_t U = -\partial_x F, \tag{C.1}$$

with $U = (\rho_1, \rho_2)^T$ and $F(U) = \frac{\sqrt{2}}{2}(\rho_1 - \kappa\rho_1\rho_2, -\rho_2 + \kappa\rho_1\rho_2)^T$. Next, we discretize the equation in space using the Lax–Friedrichs method [43] and use the Heun time-stepping in time

$$\tilde{U}_i^n = U_i^n - \Delta t\, RHS(U_i^n),$$

$$U_i^{n+1} = U_i^n + \frac{\Delta t}{2}\left(RHS(U_i^n) + RHS(\tilde{U}_i^n)\right)$$

and define

$$RHS(U_i) = -\frac{\hat{F}_{i+1/2} - \hat{F}_{i-1/2}}{\Delta x}$$

with

$$\hat{F}_{i+1/2} = \frac{F(U_{i+1}) + F(U_i)}{2} - \frac{K}{2}(U_{i+1} - U_i)$$

where $K = \cos(\theta_1)(1 + \kappa|\sin(\theta_2 - \theta_1)|)$ is the upper bound on the speed of propagation given $\rho_1, \rho_2 < 1$. Therefore, the CFL condition for the scheme above is $K\Delta t/\Delta x < 1$, and the additional diffusion introduced by the scheme is proportional to $D = K\Delta x/2$. The scheme is first order in space and second order in time, but we found that it was sufficient for our simulations. For the results presented in the body of the paper, we chose a mesh size that gave $K\Delta t/\Delta x = 0.0024$ and $D = 0.15$. We compared the numerical solutions this mesh gave to one with a new spatial discretization 10 times smaller ($\Delta x/10$). For this mesh, $K\Delta t/\Delta x = 0.024$ and $D = 0.015$, lowering the effective diffusion by a factor of 10. Additionally, the difference between the density profiles with the two different meshes (measured via the L^2 norm) was 6.55×10^{-4}, indicating the effect from the numerical diffusion is minimal and cannot account for the fact that the final discrepancy in Fig. 6 does not vanish. This can also be seen from the profiles themselves. Numerical diffusion will cause the peaks of the profiles to decrease, but this is not observed (Fig. 3A).

Appendix D. Averaging agent-based simulations

It is not immediately clear if the average agent-based simulations yields a distribution uniform in the y-direction as assumed in the analytical model (14). We tested uniformity in the y-direction using the Kolmogorov–Smirnov (KS) test and the continuous version of Kullback–Leibler (KL) divergence. All tests below were done with all rods regardless of orientation.

Fig. 8 below shows a kernel density estimate (KDE) of the combined initial rod positions with $\kappa = 0.1$ in three cases: the initial conditions over all 1000 simulations (2856000 rods), initial conditions corresponding to 10^5 simulations (2.856×10^8 rod positions), and the final distribution of rods at the end of the simulations (2856000 rods). In all three cases, there was some variability in the y-direction, with the initial conditions from 10^5 simulations appearing the most uniform, and the final rod positions from 1000 simulations appearing the least uniform. Since one of the predictions of the analytical model is that uniformity in the y-direction should be conserved, this indicated two possibilities. Either uniform initial conditions in the y-direction are unstable, or the analytical model is failing to match the agent simulations. Since the agent simulations run on the microscopic rules the analytical model was derived from, the latter would suggest this disagreement is another way in which the Boltzmann hypothesis is failing.

The rejection rates from the KS test for each of the three sets of rod positions are given in Table D.1 below. For each, the x-direction was divided into bins of equal size, and the KS test was performed on the rods in each bin. Each test resulted in either an acceptance of the null hypothesis (that the distribution is uniform in the y-direction) or

Table D.1
Results of the Kolmogorov-Smirnov test on the distribution of rods in the y-direction with various bin sizes for the x-direction. The distribution of rods in the y-direction was compared to a uniform distribution.

KS Test	400 bins	40 bins	4 bins	1 bin
IC 10^3 sims	6.25%	7.50%	0%	0%
IC 10^5 sims	4.76%	5.13%	0%	0%
FC 10^3 sims	8.25%	45%	75%	0%

Table D.2
Measurements of the Kullback-Leibler divergence on the distribution of rods in the y-direction. The KL divergence was measured for two initial conditions with 10^3 and 10^5 rods and for the final distribution of rods from the initial conditions with 10^3 rods.

	IC 10^3 sims	IC 10^5 sims	FC 10^3 sims
Average KL divergence	6×10^{-5}	3×10^{-6}	1.5×10^{-3}

a rejection. All tests were done at standard level of rejection $\alpha = 0.05$. IC indicates initial conditions, FC indicates final conditions at the end of the simulation.

The rates of rejection were slightly lower for the finest and coarsest bin sizes, but in all cases the results are the same when all rod positions are considered together. The null hypothesis is not rejected, indicating the distribution is close to uniform in the y-direction when all rods are considered together or when the rods are grouped into bins with small widths. Since the final rod positions averaged over 1000 simulations appeared the least uniform, the final KS test with all rods was redone at $\alpha = 0.1$ and $\alpha = 0.2$, corresponding to a stricter test condition. In both cases the KS test again did not reject the null hypothesis.

For the KL divergence, the KDE from each of the three cases was measured against a uniform distribution at each value of x where the KDE was calculated. The values of the divergence where then averaged over x to get an average. The results are presented in Table D.2 below. In all three cases, the divergence is quite low, indicated that from an entropic viewpoint, the KDEs resemble uniform distributions in the y-direction.

From the KDEs, the KS test, and the KL divergence, we concluded the distribution of rod positions in the y-direction is not perfectly uniform, but does resemble a uniform distribution.

Appendix E. Supplementary data

Supplementary material related to this article can be found online at https://doi.org/10.1016/j.mbs.2024.109266.

References

[1] F.J. Ndlec, T. Surrey, A.C. Maggs, S. Leibler, Self-organization of microtubules and motors, Nature 389 (6648) (1997) 305–308.
[2] Ingmar H. Riedel, Karsten Kruse, Jonathon Howard, A self-organized vortex array of hydrodynamically entrained sperm cells, Science 309 (5732) (2005) 300–303.
[3] Vijay Narayan, Sriram Ramaswamy, Narayanan Menon, Long-lived giant number fluctuations in a swarming granular nematic, Science 317 (5834) (2007) 105–108.
[4] Volker Schaller, Christoph Weber, Christine Semmrich, Erwin Frey, Andreas R. Bausch, Polar patterns of driven filaments, Nature 467 (7311) (2010) 73–77.
[5] Yutaka Sumino, Ken H. Nagai, Yuji Shitaka, Dan Tanaka, Kenichi Yoshikawa, Hugues Chaté, Kazuhiro Oiwa, Large-scale vortex lattice emerging from collectively moving microtubules, Nature 483 (7390) (2012) 448–452.
[6] Rajesh Balagam, Douglas B. Litwin, Fabian Czerwinski, Mingzhai Sun, Heidi B. Kaplan, Joshua W. Shaevitz, Oleg A. Igoshin, Myxococcus xanthus gliding motors are elastically coupled to the substrate as predicted by the focal adhesion model of gliding motility, PLoS Comput. Biol. 10 (5) (2014) e1003619.
[7] Rajesh Balagam, Oleg A. Igoshin, Mechanism for collective cell alignment in myxococcus xanthus bacteria, PLoS Comput. Biol. 11 (8) (2015) e1004474.
[8] Aparna Baskaran, M. Cristina Marchetti, Hydrodynamics of self-propelled hard rods, Phys. Rev. E 77 (1) (2008) 011920.
[9] Aparna Baskaran, M. Cristina Marchetti, Enhanced diffusion and ordering of self-propelled rods, Phys. Rev. Lett. 101 (26) (2008) 268101.
[10] Aparna Baskaran, M. Cristina Marchetti, Statistical mechanics and hydrodynamics of bacterial suspensions, Proc. Natl. Acad. Sci. USA 106 (37) (2009) 15567–15572.
[11] Dale Kaiser, Coupling cell movement to multicellular development in myxobacteria, Nat. Rev. Microbiol. 1 (1) (2003) 45–54.
[12] Yilin Wu, Yi Jiang, Dale Kaiser, Mark Alber, Social interactions in myxobacterial swarming, PLoS Comput. Biol. 3 (12) (2007) e253.
[13] Shashi Thutupalli, Mingzhai Sun, Filiz Bunyak, Kannappan Palaniappan, Joshua W. Shaevitz, Directional reversals enable myxococcus xanthus cells to produce collective one-dimensional streams during fruiting-body formation, J. R. Soc. Interface 12 (109) (2015) 20150049.
[14] E. Bertin, M. Droz, G. Grégoire, Boltzmann and hydrodynamic description for self-propelled particles, Phys. Rev. E Stat. Nonlin. Soft. Matter. Phys. 74 (2006).
[15] Pierre Degond, Angelika Manhart, Hui Yu, An age-structured continuum model for myxobacteria, Math. Models Methods Appl. Sci. 28 (09) (2018) 1737–1770.
[16] Pierre Degond, Sébastien Motsch, Continuum limit of self-driven particles with orientation interaction, Math. Models Methods Appl. Sci. 18 (supp01) (2008) 1193–1215.
[17] Sabine Hittmeir, Laura Kanzler, Angelika Manhart, Christian Schmeiser, Kinetic modelling of colonies of myxobacteria, Kinet. Relat. Models 14 (1) (2021) 1–24.
[18] Fernando Peruani, Andreas Deutsch, Markus Bär, Nonequilibrium clustering of self-propelled rods, Phys. Rev. E 74 (3) (2006) 030904.
[19] Thomas Ihle, Kinetic theory of flocking: Derivation of hydrodynamic equations, Phys. Rev. E 83 (3) (2011) 030901, Publisher: American Physical Society.
[20] François Bolley, José A. Cañizo, José A. Carrillo, Mean-field limit for the stochastic Vicsek model, Appl. Math. Lett. 25 (3) (2012) 339–343.
[21] Timo Hanke, Christoph A. Weber, Erwin Frey, Understanding collective dynamics of soft active colloids by binary scattering, Phys. Rev. E 88 (5) (2013) 052309, Publisher: American Physical Society.
[22] A. Peshkov, E. Bertin, F. Ginelli, H. Chaté, Boltzmann–Ginzburg–Landau approach for continuous descriptions of generic Vicsek-like models, Eur. Phys. J. Spec. Top. 223 (7) (2014) 1315–1344.
[23] Misha Perepelitsa, Ilya Timofeyev, Patrick Murphy, Oleg A. Igoshin, Mean-field model for nematic alignment of self-propelled rods, Phys. Rev. E 106 (3) (2022) 034613, Publisher: American Physical Society.
[24] Fernando Peruani, Andreas Deutsch, Markus Bär, A mean-field theory for self-propelled particles interacting by velocity alignment mechanisms, Eur. Phys. J. Spec. Top. 157 (2008) 111–122.
[25] F. Ginelli, F. Peruani, M. Bär, H. Chaté, Large-scale collective properties of self-propelled rods, Phys. Rev. Lett. 104 (2010).
[26] Pierre Degond, Tong Yang, Diffusion in a continuum model of self-propelled particles with alignment interaction, Math. Models Methods Appl. Sci. 20 (supp01) (2010) 1459–1490.
[27] Pierre Degond, Angelika Manhart, Hui Yu, A continuum model for nematic alignment of self-propelled particles, Discrete Contin. Dyn. Syst. - B 22 (4) (2017) 1295.
[28] Florian Thüroff, Christoph A. Weber, Erwin Frey, Critical assessment of the Boltzmann approach to active systems, Phys. Rev. Lett. 111 (19) (2013) 190601, Publisher: American Physical Society.
[29] T. Ihle, Towards a quantitative kinetic theory of polar active matter, Eur. Phys. J. Spec. Top. 223 (7) (2014) 1293–1314.
[30] Ryo Suzuki, Christoph A. Weber, Erwin Frey, Andreas R. Bausch, Polar pattern formation in driven filament systems requires non-binary particle collisions, Nat. Phys. 11 (10) (2015) 839–843, Number: 10 Publisher: Nature Publishing Group.
[31] Fernando Peruani, Jörn Starruß, Vladimir Jakovljevic, Lotte Søgaard-Andersen, Andreas Deutsch, Markus Bär, Collective motion and nonequilibrium cluster formation in colonies of gliding bacteria, Phys. Rev. Lett. 108 (9) (2012) 098102, Publisher: American Physical Society.
[32] Christoph A. Weber, Volker Schaller, Andreas R. Bausch, Erwin Frey, Nucleation-induced transition to collective motion in active systems, Phys. Rev. E 86 (3) (2012) 030901, Publisher: American Physical Society.
[33] Julian Jeggle, Joakim Stenhammar, Raphael Wittkowski, Pair-distribution function of active Brownian spheres in two spatial dimensions: Simulation results and analytic representation, J. Chem. Phys. 152 (19) (2020) 194903.
[34] Rüdiger Kürsten, Sven Stroteich, Martín Zumaya Hernández, Thomas Ihle, Multiple particle correlation analysis of many-particle systems: formalism and application to active matter, Phys. Rev. Lett. 124 (8) (2020) 088002.
[35] Rüdiger Kürsten, Thomas Ihle, Quantitative kinetic theory of flocking with three-particle closure, Phys. Rev. E 104 (3) (2021-09-03) 034604.
[36] Len Pismen, Active matter within and around us: From self-propelled particles to flocks and living forms, The Frontiers Collection, Springer International Publishing, Cham, 2021.
[37] F. Peruani, L. Schimansky-Geier, M. Bär, Cluster dynamics and cluster size distributions in systems of self-propelled particles, Eur. Phys. J. Spec. Top. 191 (1) (2010) 173–185.
[38] Christoph A. Weber, Florian Thüroff, Erwin Frey, Role of particle conservation in self-propelled particle systems, New J. Phys. 15 (4) (2013) 045014, Publisher: IOP Publishing.
[39] N.N. Bogoliubov, Kinetic equations, J. Phys. USSR 10 (1946) 265–274.
[40] Harold Grad, On the kinetic theory of rarefied gases, Comm. Pure Appl. Math. 2 (1949) 331–407.

[41] C. Cercignani, The Boltzmann Equation and Its Applications, Springer-Verlag, New York, 1988.
[42] Yen-Liang Chou, Thomas Ihle, Active matter beyond mean-field: Ring-kinetic theory for self-propelled particles, Phys. Rev. E 91 (2) (2015) 022103, Publisher: American Physical Society.
[43] R. LeVeque, Finite Volume Methods for Hyperbolic Problems, Cambridge University Press, 2002.